

# AURA : Automatic Mask Generator using Randomized Input Sampling for Object Removal

Changsuk Oh  
Seoul National University  
Department of Aerospace Engineering  
santgo@snu.ac.kr

Dongseok Shim  
Seoul National University  
Interdisciplinary Program in AI  
tlaehdtjr01@snu.ac.kr

H. Jin Kim  
Seoul National University  
Department of Aerospace Engineering  
hjinkim@snu.ac.kr

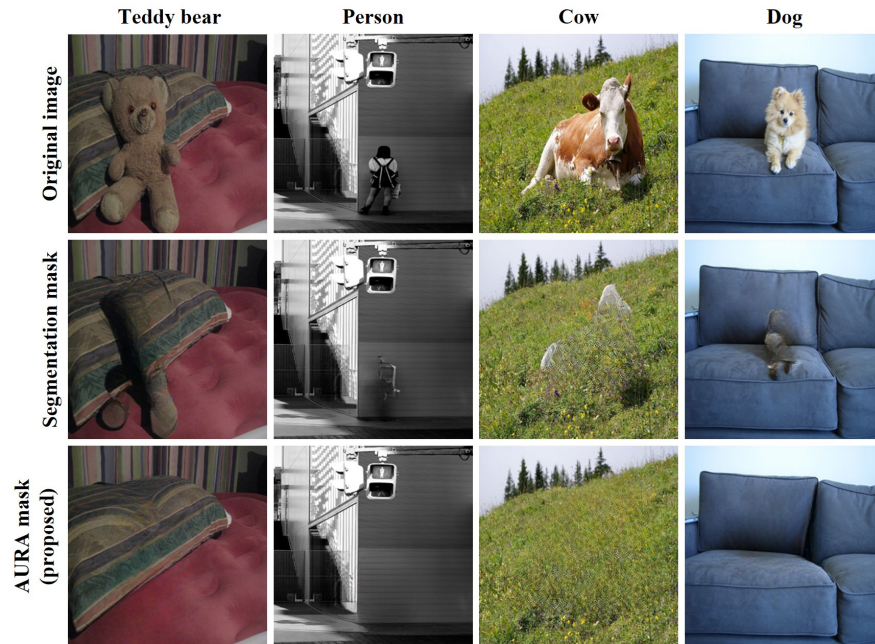


Figure 1: Object removal results on the COCO dataset.

## Abstract

The objective of the image inpainting task is to fill missing regions of an image in a visually plausible way. Recently, deep-learning-based image inpainting networks have generated outstanding results, and some utilize their models as object removers by masking unwanted objects in an image. However, while trying to better remove objects using their networks, the previous works pay less attention to the importance of the input mask. In this paper, we focus on generating the input mask to better remove objects using the off-the-shelf image inpaint-

ing network. We propose an automatic mask generator inspired by the explainable AI (XAI) method, whose output can better remove objects than a semantic segmentation mask. The proposed method generates an importance map using randomly sampled input masks and quantitatively estimated scores of the completed images obtained from the random masks. The output mask is selected by a judge module among the candidate masks which are generated from the importance map. We design the judge module to quantitatively estimate the quality of the object removal results. In addition, we empirically find that the evaluation methods used in the previous works

*reporting object removal results are not appropriate for estimating the performance of an object remover. Therefore, we propose new evaluation metrics (FID\* and U-IDS\*) to properly evaluate the quality of object removers. Experiments confirm that our method shows better performance in removing target class objects than the masks generated from the semantic segmentation maps, and the two proposed metrics make judgments consistent with humans.*

## 1. Introduction

The objective of an image inpainting network is to restore missing parts of an image plausibly. Recently, image inpainting networks [12, 2, 20, 17, 1, 34, 25, 39, 27, 36, 43, 6, 46, 14, 13, 29] have generated remarkable outputs powered by deep learning methods that have achieved outstanding success on various image domain tasks. To train data-driven image inpainting networks, training datasets are synthesized by covering masks on intact images. [35, 5, 21, 32, 33, 28, 42] and [17, 11, 18, 37, 10, 30, 26, 23, 19, 38] use rectangular- and irregular-shaped masks, respectively. And semantic segmentation masks are utilized to obtain training samples in [25, 34, 1, 2].

After training inpainting networks using the various masks, [17, 34, 1, 25, 39, 27, 38] report that their methods can be used not only to restore corrupted images but also to edit images for object removal. When a mask completely covers an object in an image, the masked image has no information about the object. Therefore, the object is not included in the restored image. Using this property, [17, 34, 1, 25, 39, 27, 38] use semantic segmentation masks or human-made masks that completely cover objects to remove them in images. However, although the above studies have reported that their methods outperform other networks under identical input (masked image), there is *no* discussion on which mask can better erase target objects using their networks.

In this paper, we propose a new mask generation method called AUTOMATIC mask generator using RANDOMIZED input sampling (AURA), which focuses on generating the input mask to better remove objects using the off-the-shelf image inpainting network. This work is inspired by the explainable AI (XAI) method [22], which tries to understand a black-box classification network’s prediction. The proposed mask generator randomly samples input masks and gets restored images using them. Then,

AURA generates an importance map. An importance of a pixel represents the expected quantitative score of the completed image when the pixel is masked. We use a weighted linear combination of random masks to generate an importance map, where the quantitative evaluations of the masks are used as scaling factors. We design the judge module to evaluate the quality of the outputs by quantifying 1) how much the afterimage of the target objects remains and 2) whether the backgrounds have been well restored. AURA generates candidate masks by masking pixels that exceed predefined percentile values of the importance map, and the judge module figures out the best mask among them. In this way, we can make the input masks for better inferences, while the existing object removers focus on the network architectures and training data synthesis. And we test our method on the COCO [16] and KITTI [3] datasets. In this paper, we evaluate an object remover highly if it preserves the original image well while leaving no visual features of the target objects to be removed.

We then study the evaluation methods for object removers. The works [25, 1, 27] reporting quantitative object removal results use evaluation methods for image inpainting networks. However, in Section 4, we empirically show that the methods are not adequate to evaluate the performance of object removers. To properly estimate the performance of object removers, we modify two existing evaluation metrics (FID [4] and U-IDS [44]) and show that the two modified metrics make judgments consistent with humans’.

This paper has the following contributions:

- This is the first paper that focuses on the input mask to better remove objects in an image using the image inpainting network.
- We propose AURA, an automatic mask generator that produces a mask which can better remove target class objects than the semantic segmentation mask and its variants (enlarged semantic segmentation masks).
- We show that the evaluation metrics used in [25, 1, 27] are not adequate to evaluate the performance of object removers. We modify two existing evaluation methods to properly evaluate the performance of object removers and verify that the modified metrics make judgments consistent with human’s judgments.

## 2. Related Work

### 2.1. Mask shapes for image inpainting networks

We need pairs of intact and corrupted images to train image inpainting networks in a supervised manner. To obtain sufficient training data, the existing works utilize various sizes and shapes of masks. Rectangular-shaped masks [35, 5, 21, 32, 33, 28, 42] and irregular-shaped masks [17, 11, 18, 37, 10, 30, 26, 23, 19, 38] are exploited to generate training data. However, the importance of input masks to make better inferences using trained inpainting networks has not been sufficiently studied. Specifically, [17, 34, 1, 25, 39, 27, 38] report object removal results using their inpainting networks. They utilize object-shaped masks to remove objects in images, and the masks are generated from semantic segmentation labels or manually drawn by humans. As mentioned earlier, however, no studies try to manipulate the input masks to better remove target objects. In this paper, we focus on the input mask to better remove objects using the off-the-shelf image inpainting network.

### 2.2. Evaluation Methods for Object Removal Task

Unlike an image generative model utilizes evaluation metrics which estimate fidelity or diversity of synthesized samples, performance of an image inpainting network is evaluated by the fidelity metrics, such as LPIPS [41], L2, P-IDS, U-IDS [44], FID [4], SSIM [31], PSNR, and PAR [40]. This is because the objective of an image inpainting network is not generating diverse and realistic samples under the trained data distribution but completing missing parts of a given image. The works [25, 1, 27] which report quantitative object removal results also exploit the fidelity metrics, e.g., FID [27, 1], PSNR [25, 1], SSIM [25, 1], LPIPS [27], L2 [25].

However, we empirically find that the above evaluation metrics used in [25, 1, 27] are inadequate to evaluate the performance of object removers. We generate target segmentation masks where only target class objects (removal targets) are labeled. We also make enlarged target segmentation masks using `opencv.dilate(kernel_size)` function. Fig. 2 shows fidelity scores of the completed images using the target segmentation mask and its variants (enlarged target segmentation mask) as input to the object remover [27]. All metrics estimate that the quality of the completed images decreases as the size of

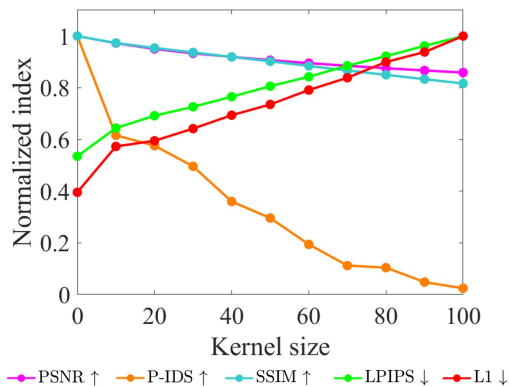


Figure 2: Evaluations of the paired data metrics. The completed images are generated by the target segmentation masks and the enlarged segmentation masks using `opencv.dilate(kernel_size)` function. We remove *person* class objects in COCO validation set. The scores of each method are divided by the highest score of each method. ↑ and ↓ indicate higher is better and lower is better, respectively.

the mask increases. However, this evaluations are inconsistent to humans’. As shown in Fig. 4(b), humans assess that the object is best erased when  $kernel\_size = 10$ . The simple experiment shows that even if the above metrics are suitable for comparing which methodology fills the missing parts more plausibly under identical inputs (i.e. masked images), they are not adequate to evaluate which mask removes objects better utilizing one inpainting network. This is because they represent the input mask size of the completed images when the completed images are generated by one inpainting network with various masks. Therefore, in Section 4, we modify some of the evaluation metrics to properly evaluate the performance of the object remover. Additionally, we show that PAR [40], a recently proposed fidelity evaluation metric for image inpainting networks, is suitable for evaluating the performance of object removers.

## 3. Method

### 3.1. Preliminary

Randomized Input Sampling for Explanation [22] generates a saliency map which shows importance of each pixel for a black-box classification network’s inference. Unlike white-box networks, an user cannot access the parameters of a black-box model. Therefore, [22] uses randomly sampled inputs (masks)

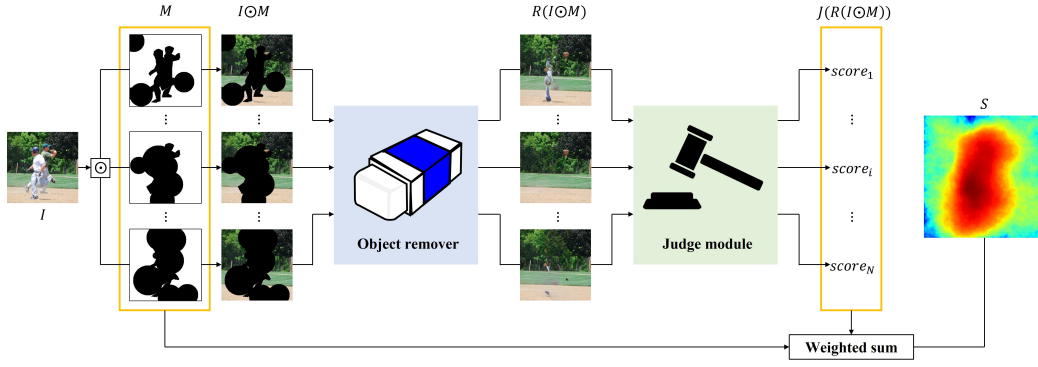


Figure 3: Flowchart of the importance map generation process.

and the outputs to understand a black-box model. Specifically, the authors define the importance of a pixel  $x \in \Omega$  as the expected confidence score when the pixel is not masked, where  $\Omega = \{1, \dots, H\} \times \{1, \dots, W\}$ . Then, the importance of a pixel can be written as

$$S_{I,f}(x) = \mathbb{E}_M [ f(I \odot M) | M(x) = 1 ], \quad (1)$$

where  $f$  represents a black-box classifier that maps an image  $I$  to a confidence score, and  $M : \Omega \mapsto \{0, 1\}$  indicates a random mask with distribution  $\mathcal{D}$ .  $\odot$  denotes the element-wise multiplication.

### 3.2. Automatic Mask Generator using Random Input Sampling

In this section, we introduce AUTOMATIC mask generator using RANdom input sampling (AURA), an automatic mask-generating method for object removal tasks. AURA makes an importance map using randomly sampled masks and completed images, which is depicted in Fig. 3. Similar to the saliency map of [22], the importance map of AURA shows the expected quality of the completed image when each pixel is masked. In other words, an object remover can more plausibly erase objects when pixels with high importance are masked. The proposed method generates candidate masks using the importance map, and the judge module selects the mask that can best remove objects among them.

**Mask Generation** We sample random masks  $\{M_1, \dots, M_N\}$  by adding patches to the target segmentation map where only target class objects are labeled. Consequently, AURA can focus on figuring out which pixels should be further masked in the segmentation map rather than searching pixels among the entire image. We randomly sample the number, size, and location of additional patches, and details

about the sampling process are presented in supplementary materials.

**Judge module** Utilizing a random mask  $M_{i \in \{1, \dots, N\}}$  and an image inpainting network (object remover)  $\mathcal{R}$ , we can obtain the completed image  $\mathcal{R}(I \odot M_i)$ . Using the judge module  $\mathcal{J}$ , AURA quantitatively evaluates how well objects in the images are removed. The evaluation scores are used as weights for a linear combination of the masks to generate the importance map. The judge module evaluates how much 1) objects remain (Eq. 2), 2) the afterimage of the target objects remains (Eq. 4), and 3) the background is deformed (Eq. 3).

The 2D object detector [24] is employed to find visual features of target class objects in the completed image. The judge module gives a low score when the objects are detected in the completed image.  $\mathcal{J}_{detect}$  is calculated as follows:

$$\mathcal{J}_{detect} = - \frac{\mathcal{A}(\mathcal{S}(\mathcal{R}(I \odot M_i)))}{\mathcal{A}(L)} \quad (2)$$

Let  $\mathcal{S} : \Omega \rightarrow \{0, 1\}$  make a binary map, which marks the detected areas as 1.  $\mathcal{A}$  counts the number of pixels whose pixel value is 1 in a binary map. Pixels from target class objects are marked as 1 in the target segmentation map  $L$ . When the size of objects is small, even if they are detected, they do not significantly affect the overall score. To properly evaluate whether objects are removed well regardless of the objects' size, the size of the target segmentation mask is divided.

$\mathcal{J}_{background}$  quantifies the similarity between the original image's background region and the completed image's corresponding region. We convert the RGB intensities of the target objects' pixels to zero.  $\mathcal{J}_{background}$  is designed to give a low score if the background of the completed image is different from

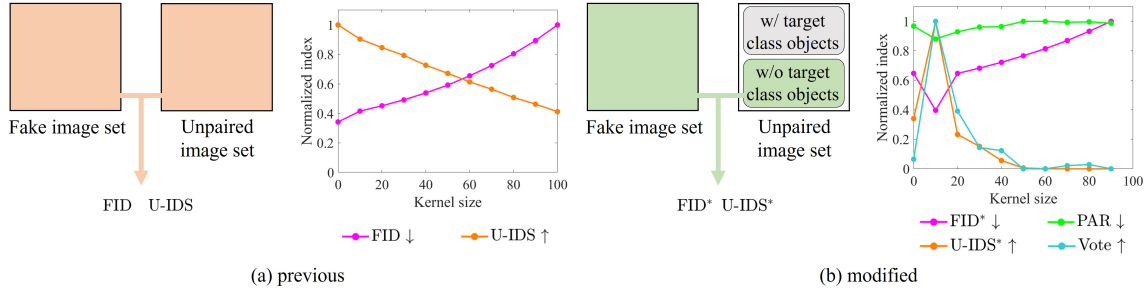


Figure 4: Evaluations of the unpaired metrics (i.e. FID and U-IDS), modified metrics (i.e. FID\* and U-IDS\*), PAR, and human evaluators (votes). The completed images are generated by the target segmentation masks and the enlarged segmentation masks using `opencv.dilate(kernel_size)` function. We remove `person` class objects in COCO validation set and utilize COCO train set images without a person as a comparison set. The scores of each method are divided by the highest score of each method.  $\uparrow$  and  $\downarrow$  indicate higher is better and lower is better, respectively.

the original image’s background. The judge module utilizes negative L2 to calculate the differences between the two manipulated images. We calculate  $\mathcal{J}_{background}$  as follows:

$$\mathcal{J}_{background} = \frac{\mathcal{L}_2(I \odot (\mathbb{1}_M - L), \mathcal{R}(I \odot M_i) \odot (\mathbb{1}_M - L))}{H \cdot W - A(L)}. \quad (3)$$

We find that a mask that tightly covers an object leaves an afterimage of the object in the completed image, as shown in Figs. 1 and 5.  $\mathcal{J}_{afterimage}$  is designed to give a low score if there is an afterimage of the target objects. It calculates the perceptual difference between the completed images using target segmentation masks and query masks. Pixel values are converted to zeros except for pixels from the target objects to focus on regions of target objects. Contrary to  $\mathcal{J}_{background}$ , we utilize LPIPS to quantify the difference between the two manipulated images. Similar to  $\mathcal{J}_{detect}$ , we divide  $\mathcal{J}_{background}$  and  $\mathcal{J}_{afterimage}$  using their respective valid areas.

$$\mathcal{J}_{afterimage} = \frac{LPIPS(\mathcal{R}(I \odot M_i) \odot L, \mathcal{R}(I \odot (\mathbb{1}_M - L)) \odot L)}{A(L)}. \quad (4)$$

The overall score function of the judge module can be summarized as

$$\mathcal{J} = \mathcal{J}_{background} + \lambda_a \mathcal{J}_{afterimage} + \lambda_d \mathcal{J}_{detect}, \quad (5)$$

where the hyper-parameters are empirically set as  $\lambda_a = 90,000$  and  $\lambda_d = 0.5$ .

**Importance Map** We define the importance of a pixel ( $x$ ) as the expected judge score when the pixel is masked ( $M(x) = 0$ ). The importance map ( $\Phi$ ) of AURA are expressed as

$$\Phi_{I,\mathcal{R}}(x) = \mathbb{E}_M[\mathcal{J}(\mathcal{R}(I \odot M)) | M(x) = 0] \quad (6)$$

We follow [22] to approximate the conditional expectation using Monte Carlo sampling as follows:

$$\Phi_{I,\mathcal{R}} \approx \frac{\sum_{i=1}^N \mathcal{J}(\mathcal{R}(I \odot M_i)) \cdot (\mathbb{1}_M - M_i)}{N \cdot \mathbb{1}_M - \sum_{j=1}^N M_j} \quad (7)$$

Further details about how we calculate the importance map are presented in supplementary materials.

**Candidate mask generation** AURA generates candidate masks  $C$  using predefined percentiles  $P = \{x \in \mathbb{N} | 1 \leq x \leq p\}$ . Let  $\mathcal{T}$  be a function that finds the  $100 - P_j$ -th percentile score ( $\phi_j$ ) of an importance map as follows:

$$\phi_j = \mathcal{T}(\Phi, 100 - P_j) \quad (8)$$

As AURA figures out which pixels need to be further masked in the target segmentation mask, the percentage of the segmented area of the target segmentation mask is added to the percentiles.

$$\phi_j = \mathcal{T}\left(\Phi, 100 - P_j - \frac{A(L)}{H \cdot W} \cdot 100\right) \quad (9)$$

Then, the  $j$ -th candidate mask  $C_j$  is obtained by masking pixels whose importance is greater or equal

to the percentile score ( $\phi_j$ ).

$$C_j(x) = \begin{cases} 1 & \text{if } \Phi(x) \geq \phi_j \\ 0 & \text{if } \Phi(x) < \phi_j \end{cases} \quad (10)$$

Finally, AURA selects the output mask ( $C^*$ ) with the highest score evaluated by the judge module among the candidate masks:

$$C^* = \arg \max_{C_j} \mathcal{J}(\mathcal{R}(I \odot C_j)), \quad (11)$$

where  $j \in P$ .

## 4. Evaluation Metric

We can divide evaluation metrics that measure the fidelity of images into three groups. PSNR, SSIM, L2, LPIPS, and P-IDS require a pair of original and completed images, while FID and U-IDS can be measured using unpaired data. And PAR does not use a comparison image set.

For the paired data metrics, as they evaluate how similar a completed image is to the original image, the estimated quality of the completed image is inversely proportional to the size of the input mask, as shown in Fig. 2. Interestingly, we observe the inversely proportional tendency using the unpaired metrics (FID, U-IDS), as shown in Fig. 4(a). Contrary to the reputation that unpaired metrics make the assessment consistent with the humans', FID and U-IDS evaluate that the objects are best erased when  $kernel\_size = 0$ , while humans choose  $kernel\_size = 10$  as best, as shown in Fig. 4(b). We confirm that only PAR makes judgments consistent with humans'. However, we find that PAR is not suitable for evaluating object removal performance of images obtained from virtual environments. This is because PAR is trained to detect perceptual artifacts in realistic images, which limits the style of the images that PAR can evaluate. The qualitative results supporting this are presented in supplementary materials.

We modify the unpaired metrics (FID and U-IDS) to evaluate the performance of the object removers. The unpaired metrics can assess the performance of an inpainting network regardless of a query set's image style when the styles of the comparison set and query set are identical. We add a condition to the comparison set of unpaired metrics that target class objects should not be included in the comparison set, and confirm that the modified metrics make judgments which are consistent with evaluations made by humans and PAR.

Both FID and U-IDS use the pre-trained CNNs to convert images into activation vectors and evaluate the quality using them. As the existing unpaired data metrics usually do not place any restrictions on the images of the comparison set, the features from the target objects implicitly permeate the activation vectors when there are images containing the target class objects in the comparison set. Then, even if the objects are less erased and their afterimage remains in the completed images, the existing metrics cannot lower the score of the completed images with respect to the afterimage because the activation vectors of the comparison set have similar features. Therefore, the existing unpaired metrics are not adequate for evaluating the quality of object removers.

To properly evaluate object removal quality, we collect images without target class objects and use the image set to calculate FID and U-IDS. FID and U-IDS using the control group are called as FID\* and U-IDS\*. Both modified metrics evaluate that objects are best erased when  $kernel\_size = 10$ , which is consistent with the human's and PAR's evaluations, as shown in Fig. 4(b). As the activation vectors of the comparison group do not have features of the target class objects, difference from the comparison group occurs when the target object features remain in the completed images. For this reason, we infer that the two modified metrics make judgments consistent with humans'.

## 5. Experiments and Results

### 5.1. AURA w/ Semantic Segmentation Label

We conduct object removal experiments on the COCO dataset. The proposed method utilizes 2000 samples per image. We use Alexnet [8] to calculate LPIPS. The image inpainting network [27] trained on the PLACE [45] and CelebA-HQ [7] is employed as an object remover. Similar to [1], we use images whose target segmentation masks cover 5-40% of the images. We use 20 as the largest percentile ( $p$ ).

**Qualitative evaluation** Figs. 1 and 5 show the qualitative results. We can confirm that AURA masks remove target class objects in the most visually plausible manner. As shown in both figures, the afterimage of objects remains in the completed images when using the target segmentation masks that tightly cover objects. Even if we use the masks (segmentation mask using  $opencv.dilate(kernel\_size = 10)$ ) that erase objects best among the variants of the target segmentation map, it is difficult to say that the target class

Mask		airplane	cat	cow	dog	fire hydrant	horse	person	teddy bear	Votes
Segmentation	kernel_size = 0	170.63 / 6.52	99.34 / 3.41	159.64 / 2.38	102.03 / 3.15	187.56 / 2.21	123.51 / 3.71	74.37 / 3.00	144.61 / 3.43	10
	kernel_size = 10	168.70 / 4.51	91.31 / 2.98	158.70 / 2.11	93.94 / 2.72	182.40 / 1.86	120.41 / 3.52	45.63 / 2.73	134.62 / 2.86	72
AURA	proposed	<b>163.66 / 4.01</b>	<b>90.29 / 2.46</b>	<b>155.28 / 2.06</b>	<b>92.46 / 2.48</b>	<b>182.28 / 1.75</b>	<b>119.38 / 3.18</b>	<b>44.60 / 2.59</b>	<b>133.14 / 2.66</b>	<b>158</b>

Table 1: Object removal performance of segmentation masks and AURA masks. We report FID\* / PAR (in %) results on the COCO dataset. We remove the target class objects in the images of the COCO validation set. Images without each target class objects are utilized as a comparison set. The results using segmentation masks with the larger kernel size are presented in supplementary materials.

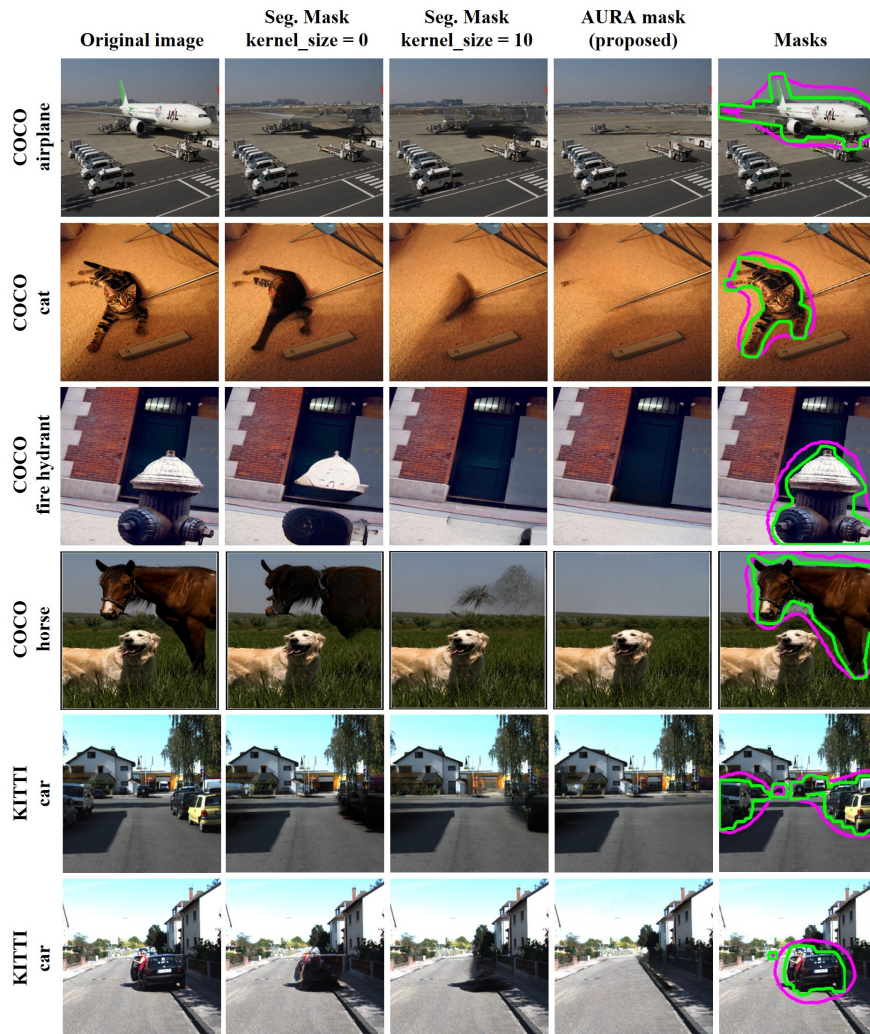


Figure 5: Object removal results on the COCO and KITTI dataset images. Green and magenta lines indicate segmentation masks using  $opencv.dilate(kernel\_size = 10)$  and AURA masks, respectively.

objects are erased well because the afterimage of the objects still remains.

**Quantitative evaluation** We compare the proposed method with the segmentation masks and their variants using the modified metrics (FID\* and U-IDS\*) and PAR. We remove objects of a target class

in the images of the COCO validation set and make the comparison image set using validation set images without the target class. In terms of FID\* and PAR, the AURA mask best removes objects in the images of *all* classes (Table 1). As our experiment uses large masks as input, the number of samples

Comparison set	Seg. mask kernel size= 0	Seg. mask kernel size = 10	AURA mask (proposed)
Train set w/o person	0.1167	0.1295	<b>0.1301</b>
Val. set w/o person	0.1205	0.1325	<b>0.1348</b>

Table 2: U-IDS\* results on the COCO dataset. *person* class objects are removed in the images of the COCO validation set. We use the COCO validation and train set images without the *person* class objects as the comparison set, respectively.

Mask	Seg. mask kernel size= 0	Seg. mask kernel size = 10	AURA mask (proposed)
FID* / PAR	78.77 / 1.45	63.87 / 1.28	<b>61.43 / 1.21</b>

Table 3: FID\* and PAR (in %) results on the KITTI dataset. We remove objects of *car*, *truck*, and *van* classes in the images of the KITTI object detection dataset (test set). Images of the KITTI 360 dataset without the target classes objects are utilized as a comparison set. The results using segmentation masks with the larger kernel size are presented in supplementary materials.

should be more than 10K to properly evaluate the image set quality using U-IDS\*. This is because U-IDS evaluates the image set quality using a support vector machine, which can easily distinguish generated (fake) samples from real samples if the number of fake samples is small. Therefore, only object removal results of *person* class (more than 12K samples) can be properly evaluated using the U-IDS\*, and the result is presented in Table 2. We calculate U-IDS\* twice using two comparison sets (train set images and validation set images without a person). Similar to the FID\* and PAR results, the completed images using the AURA masks show the best quality.

**Human Judgment** We conduct two user studies to acquire human judgments on which mask best removes objects in an image. In the first user study, we survey which mask best removes target class objects among the variants of the target segmentation mask. 23 users are asked to choose one of the eleven images that the target class objects of the original image are removed in the most plausibly way. Each user evaluates 10 image sets, and the evaluations are presented in Fig. 4(b). The users evaluated that the objects are best removed when  $kernel\_size = 10$ . In the second study, we ask 20 users to find the best one of the three images. We make three completed images using AURA, the target segmentation mask, and the enlarged target segmentation mask us-

ing  $kernel\_size = 10$ . A user makes 12 decisions, and the results are presented in the last column of Table 1. Human judgments are consistent with the evaluation made by FID\*, U-IDS\*, and PAR. In other words, four different evaluation methods make the identical assessment that the AURA mask can better remove the target class objects than the segmentation mask and its variants.

## 5.2. AURA w/o Semantic Segmentation Label

We automatically generate masks without semantic segmentation annotations to imitate a general image editing scenario where we do not have the semantic segmentation label of an original image. We use identical parameters of the judge module used in Section 5.1. We remove the cars in the images of the KITTI object detection dataset, which does not have semantic segmentation annotations. Our method uses the estimated semantic segmentation map from the pre-trained semantic segmentation network [9]. We use the network to mimic the general scenario because the network has *not* been trained on the KITTI data, and it can properly work on the unseen images as it is trained on the Mseg dataset [9], which is the largest semantic segmentation dataset with more than 200 labeled classes. The qualitative results are presented in Fig. 5. We can easily find artifacts in the regions where the cars are located in the completed images using the segmentation masks. However, when the remover uses AURA masks, the regions are restored in a visually plausible way. We also quantitatively compare the quality of the images. In terms of FID\* and PAR, our method excels the others. We use images without cars of the KITTI 360 dataset [15] as the comparison set.

## 6. Conclusion

We propose an automatic mask generation method to better remove target class objects using the image inpainting network. Experiments show that our method can better remove objects not only when there are semantic segmentation labels of the images but also for the images without the semantic segmentation labels. Further, we show that the modified evaluation methods for object removers make consistent judgments to humans’, which indicates that FID\* and U-IDS\* can properly evaluate the performance of object removers.



## References

- [1] Chenjie Cao and Yanwei Fu. Learning a sketch tensor space for image inpainting of man-made scenes. In *Proceedings of the IEEE/CVF International Conference on Computer Vision*, pages 14509–14518, 2021. [2](#), [3](#), [6](#)
- [2] Qiaole Dong, Chenjie Cao, and Yanwei Fu. Incremental transformer structure enhanced image inpainting with masking positional encoding. In *Proceedings of the IEEE/CVF Conference on Computer Vision and Pattern Recognition*, pages 11358–11368, 2022. [2](#)
- [3] Andreas Geiger, Philip Lenz, and Raquel Urtasun. Are we ready for autonomous driving? the kitti vision benchmark suite. In *Conference on Computer Vision and Pattern Recognition (CVPR)*, 2012. [2](#)
- [4] Martin Heusel, Hubert Ramsauer, Thomas Unterthiner, Bernhard Nessler, and Sepp Hochreiter. Gans trained by a two time-scale update rule converge to a local nash equilibrium. *Advances in neural information processing systems*, 30, 2017. [2](#), [3](#)
- [5] Satoshi Iizuka, Edgar Simo-Serra, and Hiroshi Ishikawa. Globally and locally consistent image completion. *ACM Transactions on Graphics (TOG)*, 36(4):1–14, 2017. [2](#), [3](#)
- [6] Jireh Jam, Connah Kendrick, Vincent Drouard, Kevin Walker, Gee-Sern Hsu, and Moi Hoon Yap. R-mnet: A perceptual adversarial network for image inpainting. In *Proceedings of the IEEE/CVF Winter Conference on Applications of Computer Vision*, pages 2714–2723, 2021. [2](#)
- [7] Tero Karras, Timo Aila, Samuli Laine, and Jaakko Lehtinen. Progressive growing of gans for improved quality, stability, and variation. *arXiv preprint arXiv:1710.10196*, 2017. [6](#)
- [8] Alex Krizhevsky. One weird trick for parallelizing convolutional neural networks. *arXiv preprint arXiv:1404.5997*, 2014. [6](#)
- [9] J. Lambert et al. Mseg: A composite dataset for multi-domain semantic segmentation. In *CVPR*, 2020. [8](#)
- [10] Chu-Tak Li, Wan-Chi Siu, Zhi-Song Liu, Li-Wen Wang, and Daniel Pak-Kong Lun. Deepgin: Deep generative inpainting network for extreme image inpainting. In *Computer Vision–ECCV 2020 Workshops: Glasgow, UK, August 23–28, 2020, Proceedings, Part IV 16*, pages 5–22. Springer, 2020. [2](#), [3](#)
- [11] Jingyuan Li, Ning Wang, Lefei Zhang, Bo Du, and Dacheng Tao. Recurrent feature reasoning for image inpainting. In *Proceedings of the IEEE/CVF Conference on Computer Vision and Pattern Recognition*, pages 7760–7768, 2020. [2](#), [3](#)
- [12] Wenbo Li, Zhe Lin, Kun Zhou, Lu Qi, Yi Wang, and Jiaya Jia. Mat: Mask-aware transformer for large hole image inpainting. In *Proceedings of the IEEE/CVF Conference on Computer Vision and Pattern Recognition*, pages 10758–10768, 2022. [2](#)
- [13] Xiaoguang Li, Qing Guo, Di Lin, Ping Li, Wei Feng, and Song Wang. Misf: Multi-level interactive siamese filtering for high-fidelity image inpainting. In *Proceedings of the IEEE/CVF Conference on Computer Vision and Pattern Recognition (CVPR)*, pages 1869–1878, June 2022. [2](#)
- [14] Liang Liao, Jing Xiao, Zheng Wang, Chia-Wen Lin, and Shin’ichi Satoh. Image inpainting guided by coherence priors of semantics and textures. In *Proceedings of the IEEE/CVF Conference on Computer Vision and Pattern Recognition*, pages 6539–6548, 2021. [2](#)
- [15] Yiyi Liao, Jun Xie, and Andreas Geiger. Kitti-360: A novel dataset and benchmarks for urban scene understanding in 2d and 3d. *IEEE Transactions on Pattern Analysis and Machine Intelligence*, 2022. [8](#)
- [16] Tsung-Yi Lin, Michael Maire, Serge Belongie, James Hays, Pietro Perona, Deva Ramanan, Piotr Dollár, and C Lawrence Zitnick. Microsoft coco: Common objects in context. In *European conference on computer vision*, pages 740–755. Springer, 2014. [2](#)
- [17] Guilin Liu, Fitsum A Reda, Kevin J Shih, Ting-Chun Wang, Andrew Tao, and Bryan Catanzaro. Image inpainting for irregular holes using partial convolutions. In *Proceedings of the European conference on computer vision (ECCV)*, pages 85–100, 2018. [2](#), [3](#)
- [18] Hongyu Liu, Ziyu Wan, Wei Huang, Yibing Song, Xintong Han, and Jing Liao. Pd-gan: Probabilistic diverse gan for image inpainting. In *Proceedings of the IEEE/CVF Conference on Computer Vision and Pattern Recognition*, pages 9371–9381, 2021. [2](#), [3](#)
- [19] Qiankun Liu, Zhentao Tan, Dongdong Chen, Qi Chu, Xiyang Dai, Yinpeng Chen, Mengchen Liu, Lu Yuan, and Nenghai Yu. Reduce information loss in transformers for pluralistic image inpainting. In *Proceedings of the IEEE/CVF Conference on Computer Vision and Pattern Recognition*, pages 11347–11357, 2022. [2](#), [3](#)
- [20] Andreas Lugmayr, Martin Danelljan, Andres Romero, Fisher Yu, Radu Timofte, and Luc Van Gool. Repaint: Inpainting using denoising diffusion probabilistic models. In *Proceedings of the IEEE/CVF Conference on Computer Vision and Pattern Recognition*, pages 11461–11471, 2022. [2](#)
- [21] Deepak Pathak, Philipp Krahenbuhl, Jeff Donahue, Trevor Darrell, and Alexei A Efros. Context encoders: Feature learning by inpainting. In *Proceedings of the IEEE conference on computer vision and pattern recognition*, pages 2536–2544, 2016. [2](#), [3](#)
- [22] Vitali Petsiuk, Abir Das, and Kate Saenko. Rise: Randomized input sampling for explanation of black-box models. In *Proceedings of the British Machine Vision Conference (BMVC)*, 2018. [2](#), [3](#), [4](#), [5](#)

- [23] Weize Quan, Ruisong Zhang, Yong Zhang, Zhifeng Li, Jue Wang, and Dong-Ming Yan. Image inpainting with local and global refinement. *IEEE Transactions on Image Processing*, 31:2405–2420, 2022. 2, 3
- [24] Joseph Redmon and Ali Farhadi. Yolov3: An incremental improvement. *arXiv preprint arXiv:1804.02767*, 2018. 4
- [25] Robin Rombach, Andreas Blattmann, Dominik Lorenz, Patrick Esser, and Björn Ommer. High-resolution image synthesis with latent diffusion models. In *Proceedings of the IEEE/CVF Conference on Computer Vision and Pattern Recognition*, pages 10684–10695, 2022. 2, 3
- [26] Yong-Goo Shin, Min-Cheol Sagong, Yoon-Jae Yeo, Seung-Wook Kim, and Sung-Jea Ko. Pepsi++: Fast and lightweight network for image inpainting. *IEEE transactions on neural networks and learning systems*, 32(1):252–265, 2020. 2, 3
- [27] Roman Suvorov, Elizaveta Logacheva, Anton Mashikhin, Anastasia Remizova, Arsenii Ashukha, Aleksei Silvestrov, Naejin Kong, Harshith Goka, Kiwoong Park, and Victor Lempitsky. Resolution-robust large mask inpainting with fourier convolutions. In *Proceedings of the IEEE/CVF Winter Conference on Applications of Computer Vision*, pages 2149–2159, 2022. 2, 3, 6
- [28] Qiang Wang, Huijie Fan, Gan Sun, Yang Cong, and Yandong Tang. Laplacian pyramid adversarial network for face completion. *Pattern Recognition*, 88:493–505, 2019. 2, 3
- [29] Wentao Wang, Li Niu, Jianfu Zhang, Xue Yang, and Liqing Zhang. Dual-path image inpainting with auxiliary gan inversion. In *Proceedings of the IEEE/CVF Conference on Computer Vision and Pattern Recognition (CVPR)*, pages 11421–11430, June 2022. 2
- [30] Yi Wang, Ying-Cong Chen, Xin Tao, and Jiaya Jia. Vcnnet: A robust approach to blind image inpainting. In *Computer Vision–ECCV 2020: 16th European Conference, Glasgow, UK, August 23–28, 2020, Proceedings, Part XXV 16*, pages 752–768. Springer, 2020. 2, 3
- [31] Zhou Wang, Alan C Bovik, Hamid R Sheikh, and Eero P Simoncelli. Image quality assessment: from error visibility to structural similarity. *IEEE transactions on image processing*, 13(4):600–612, 2004. 3
- [32] Zhaoyi Yan, Xiaoming Li, Mu Li, Wangmeng Zuo, and Shiguang Shan. Shift-net: Image inpainting via deep feature rearrangement. In *Proceedings of the European Conference on Computer Vision (ECCV)*, September 2018. 2, 3
- [33] Chao Yang, Xin Lu, Zhe Lin, Eli Shechtman, Oliver Wang, and Hao Li. High-resolution image inpainting using multi-scale neural patch synthesis. In *Proceedings of the IEEE Conference on Computer Vision and Pattern Recognition (CVPR)*, July 2017. 2, 3
- [34] Zili Yi, Qiang Tang, Shekoofeh Azizi, Daesik Jang, and Zhan Xu. Contextual residual aggregation for ultra high-resolution image inpainting. In *Proceedings of the IEEE/CVF Conference on Computer Vision and Pattern Recognition*, pages 7508–7517, 2020. 2, 3
- [35] Jiahui Yu, Zhe Lin, Jimei Yang, Xiaohui Shen, Xin Lu, and Thomas S Huang. Generative image inpainting with contextual attention. In *Proceedings of the IEEE conference on computer vision and pattern recognition*, pages 5505–5514, 2018. 2, 3
- [36] Jiahui Yu, Zhe Lin, Jimei Yang, Xiaohui Shen, Xin Lu, and Thomas S Huang. Free-form image inpainting with gated convolution. In *Proceedings of the IEEE/CVF international conference on computer vision*, pages 4471–4480, 2019. 2
- [37] Yingchen Yu, Fangneng Zhan, Shijian Lu, Jianxiong Pan, Feiying Ma, Xuansong Xie, and Chunyan Miao. Wavefill: A wavelet-based generation network for image inpainting. In *Proceedings of the IEEE/CVF International Conference on Computer Vision (ICCV)*, pages 14114–14123, October 2021. 2, 3
- [38] Yanhong Zeng, Jianlong Fu, Hongyang Chao, and Baining Guo. Aggregated contextual transformations for high-resolution image inpainting. *IEEE Transactions on Visualization and Computer Graphics*, 2022. 2, 3
- [39] Yu Zeng, Zhe Lin, Jimei Yang, Jianming Zhang, Eli Shechtman, and Huchuan Lu. High-resolution image inpainting with iterative confidence feedback and guided upsampling. In *European conference on computer vision*, pages 1–17. Springer, 2020. 2, 3
- [40] Lingzhi Zhang, Yuqian Zhou, Connelly Barnes, Sohrab Amirghodsi, Zhe Lin, Eli Shechtman, and Jianbo Shi. Perceptual artifacts localization for inpainting. In *Computer Vision–ECCV 2022: 17th European Conference, Tel Aviv, Israel, October 23–27, 2022, Proceedings, Part XXIX*, pages 146–164. Springer, 2022. 3
- [41] Richard Zhang, Phillip Isola, Alexei A Efros, Eli Shechtman, and Oliver Wang. The unreasonable effectiveness of deep features as a perceptual metric. In *Proceedings of the IEEE conference on computer vision and pattern recognition*, pages 586–595, 2018. 3
- [42] Xian Zhang, Xin Wang, Canghong Shi, Zhe Yan, Xiaojie Li, Bin Kong, Siwei Lyu, Bin Zhu, Jiancheng Lv, Youbing Yin, et al. De-gan: Domain embedded gan for high quality face image inpainting. *Pattern Recognition*, 124:108415, 2022. 2, 3
- [43] Lei Zhao, Qihang Mo, Sihuan Lin, Zhizhong Wang, Zhiwen Zuo, Haibo Chen, Wei Xing, and Dongming Lu. Uctgan: Diverse image inpainting based on unsupervised cross-space translation. In *Proceedings*

- of the IEEE/CVF conference on computer vision and pattern recognition*, pages 5741–5750, 2020. [2](#)
- [44] Shengyu Zhao, Jonathan Cui, Yilun Sheng, Yue Dong, Xiao Liang, Eric I Chang, and Yan Xu. Large scale image completion via co-modulated generative adversarial networks. *arXiv preprint arXiv:2103.10428*, 2021. [2](#), [3](#)
- [45] Bolei Zhou, Agata Lapedriza, Aditya Khosla, Aude Oliva, and Antonio Torralba. Places: A 10 million image database for scene recognition. *IEEE transactions on pattern analysis and machine intelligence*, 40(6):1452–1464, 2017. [6](#)
- [46] Yuqian Zhou, Connelly Barnes, Eli Shechtman, and Sohrab Amirghodsi. Transfill: Reference-guided image inpainting by merging multiple color and spatial transformations. In *Proceedings of the IEEE/CVF conference on computer vision and pattern recognition*, pages 2266–2276, 2021. [2](#)